ARTICLE

In Vivo Delivery of Silica Nanorattle Encapsulated Docetaxel for Liver Cancer Therapy with Low Toxicity and High Efficacy

Linlin Li,[†] Fangqiong Tang,[†,*] Huiyu Liu,[†] Tianlong Liu,[†] Nanjing Hao,[†] Dong Chen,[‡,*] Xu Teng,[§] and Junqi He[§]

[†]Laboratory of Controllable Preparation and Application of Nanomaterials, Technical Institute of Physics and Chemistry, Chinese Academy of Sciences (CAS), Beijing 100190, China, [‡]Beijing Creative Nanophase Hi-Tech Company, Ltd., Beijing 100086, China, and [§]Department of Biochemistry and Molecular, School of Basic Medical Sciences, Capital Medical University, Beijing 100069, China

ABSTRACT Mesoporous silica nanomaterial is one of the most promising candidates as drug carrier for cancer therapy. Herein, *in vitro* and *in vivo* study of silica nanorattle (SN) with mesoporous and rattle-type structure as a drug delivery system was first reported. Hydrophobic antitumor drug docetaxel (Dtxl) was loaded into the PEGylated silica nanorattle (SN-PEG) with a diameter of 125 nm *via* electrostatic absorption. In human liver cancer cell Hep-G2, the half-maximum inhibiting concentration (IC_{50}) of silica nanorattle encapsulated docetaxel (SN-PEG-Dtxl) was only 7% of that of free Dtxl at 72 h. *In vivo* toxicity assessment showed that both nanocarrier of silica nanorattle (40 mg/kg, single dose) and SN-PEG-Dtxl (20 mg/kg of Dtxl, three doses) had low systematic toxicity in healthy ICR mice. The SN-PEG-Dtxl (20 mg/kg, intravenously) showed greater antitumor activity with about 15% enhanced tumor inhibition rate compared with Taxotere on the marine hepatocarcinoma 22 subcutaneous model. The results prove that the SN-PEG-Dtxl has low toxicity and high therapy efficacy, which provides convincing evidence for the silica nanorattle as a promising candidate for a drug delivery system.

KEYWORDS: silica · mesoporous · hollow · drug delivery · docetaxel · liver cancer

The past decade has witnessed a renewed interest in mesoporous silica nanomaterials (MSNs) for biomedical applications especially for cancer therapy. Compared with conventional organic carriers, the unique properties of MSNs, including large specific surface area and pore volume, tailored mesoporous structure, high chemical and mechanical stability, and favorable biocompatibility, endow them with fascinating performances as an intelligent drug delivery system.[1−4] Functionalized MSNs have been used as robust drug carriers for on-demand drug release, co-delivery of two kinds of therapeutic agents, encapsulation of hydrophobic anticancer drugs, and so on.[5−10] It is worth noting that MSNs with hollow and rattle structure show particularly higher drug loading efficiency because the interstitial hollow space can selectively and efficiently accommodate drug molecules.[11−14]

Many intelligent drug delivery systems based on MSNs have been designed; however, there have been few reports for *in vivo* cancer therapy on animal models.[15] We are relatively ignorant about the *in vivo* behavior and therapy efficacy of MSN. As known, although the *in vitro* studies are somewhat relevant with the *in vivo* ones, the complicated environment *in vivo* could not be totally mimicked.[16,17] One example is that the nanoparticles would encounter the biological barriers of opsonization once systematically administrated.[18,19] How the designed stealth nanoparticles escape the capture of mononuclear phagocytic system (MPS) to get a reasonable period of circulation time should be carefully examined *in vivo*. Another important issue is to evaluate the targeting efficiency including active targeting by ligand bioconjugation[10,20] and passive targeting by effective enhanced permeability and retention (EPR) effect,[21,22] which is difficult to mimic *in vitro*. In addition, alteration of the pharmacokinetics and biodistribution after the drug was encapsulated into the nanocarrier, as well as the relationship between the dose and systematic response of the formulation compared with free drug, must be considered *in vivo*. Attributed to all of these *in vivo* complexities, it is not surprising when well-established formulation would not show expected therapy efficacy *in vivo*. Only systematic evaluation shows irrefutable evidence that the formulation is safe and effective, and clinical translation can be permitted. So, it is critical to assess the *in vivo* toxicity and evaluate the *in vivo* therapy efficacy for the well-designed candidates of drug delivery systems.

*Address correspondence to tangfq@mail.ipc.ac.cn, creative.nanophase@gmail.com.

Received for review April 28, 2010 and accepted October 18, 2010.

Published online October 25, 2010. 10.1021/nn100918a

Recently, we reported a selective-etching method to synthesize silica nanorattles (SNs).[23] Several advantages make the silica nanorattles a suitable drug delivery system. First, the silica nanorattles have hollow and mesoporous structure. Drug molecules with suitable size and spatial structure can be absorbed into the pores and the interstitial hollow space of SN with high drug loading amount. Second, once synthesized, the silica nanorattles have amino groups on the surface, facilitating the surface functionalization and bioconjugation with biomolecules. Third, the silica nanorattles have controllable size and narrow size distribution. Silica nanorattles with suitable size can escape the clearance of MPS, have long circulation time, and can effectively accumulate in the tumor *via* EPR effect. The monodispersity of the nanomaterials ensures controllable *in vivo* biodistribution and reproducible experimental results. Fourth, fluorescent molecules can be doped into the inner core of the silica nanorattles. The fluorescent SNs with high fluorescent stability could be directly monitored when delivering the therapeutic drugs. Fifth, it can be synthesized for as high as 10 g in one reaction. The large-scale synthesis permits its future bioapplications. In this study, the silica nanorattles were first developed as a drug delivery system for the hydrophobic antitumor drug docetaxel for *in vitro* and *in vivo* liver cancer therapy. The *in vitro* study of Hep-G2 cells and *in vivo* study of the marine hepatocarcinoma 22 subcutaneous model proves that the silica nanorattle encapsulated docetaxel has reduced toxicity and enhanced therapeutic efficacy.

RESULTS AND DISCUSSION

The silica nanorattles were synthesized with a two-step selective-etching method as reported.[23] First, organic−inorganic hybrid silica nanoparticle of three layers were synthesized *via* the modified Stöber reaction with condensation of tetraethylorthosilane (TEOS) and *N*-[3-(trimethoxysilyl)propyl]ethylenediamine (TSD). Subsequently, hydrofluoric acid was used to structurally etch the middle layer of the hybrid silica nanoparticles to form silica nanorattles with mesoporous and rattle structure. Silica nanorattle with a moderate size of 125 nm was chosen to comply for the size range of EPR effect (Figure 1). The SNs were PEGylated to increase the dispersion stability and avoid aggregation of the SNs in the bloodstream by spatial repulsion between the particles. Meanwhile, PEGylation can reduce the opsonization and prolong the blood circulation. It is reported that, with covalently bound PEG chains, nanoparticles achieve longer blood circulation half-lives than the counterpart with only surface-absorbed PEG.[24,25] So here, the SNs were PEGylated (SN-PEG) by directly reacting with succinimidyl carbonate activated PEG derivatives of mPEG-SC (methoxy-poly(ethylene glycol)succinimidyl carbonate) (5000 Da) *via* coupling with the amino groups on the surface of

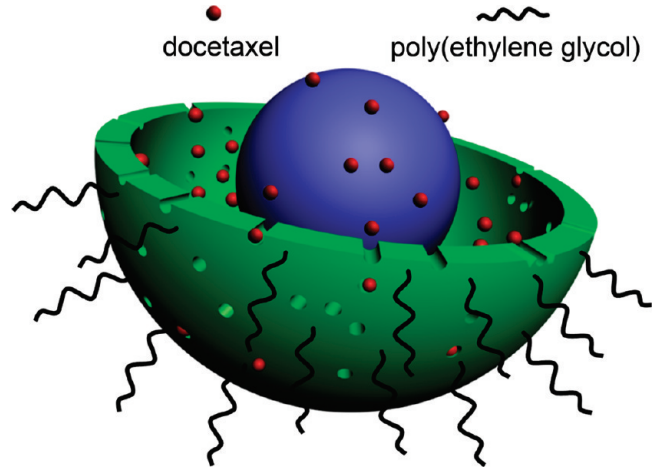

Figure 1. Schematic diagram of the drug delivery system based on silica nanorattles.

SNs. The hydrophobic antitumor drug docetaxel, which has broad effectiveness against advanced breast carcinoma, ovarian cancer, prostate cancer, and nonsmall cell lung cancer,[26] was loaded into the silica nanorattles. With an appropriate solvent to simultaneously dissolve Dtxl and disperse SN-PEG, the drug molecule of Dtxl can be electrostatically absorbed in the pore of the shell and into the hollow cavity of the silica nanorattles.

The synthesized 125 nm silica nanorattles had narrow size distribution (Figure 2A). After PEGylation with mPEG-SC, the morphology and diameter of the particles had no obvious change (Figure 2B). The hydrodynamic diameter determined by dynamic light scattering (DLS) after PEGylation was increased from 145 to 152 nm (Figure 2C). After PEGylation, the polydispersity of the nanorattle slightly increased from 0.04 to 0.09, which was still monodispersed. The SN-PEG suspension was very stable. It was not sedimented in media including water, saline, 5% glucose, and DMEM cell culture media for as long as 1 month. For drug loading, the SN-PEG was soaked in 40 mg/mL ethanol solution of Dtxl for 24 h, and then the unabsorbed drug and organic solvent were removed to obtain Dtxl-loaded SN-PEG, denoted as SN-PEG-Dtxl. The drug loading amount of SN-PEG-Dtxl was as high as 32% (48 mg Dtxl/100 mg SN-PEG). Figure 2D shows the cumulative drug release of Dtxl from the SN-PEG-Dtxl at physiological pH and temperature. It exhibited a low initial burst release (within 10% of the loaded amount) within 60 min and a two-phase drug release behavior. The initial rapid release rate in 0−20 h was attributed to the drugs weakly interacting on the outside of the silica nanorattles, and further sustained release with a lower release rate from 20 h to 5 days was attributed to the drugs being electrostatically absorbed in the mesopores and located in the hollow space of the silica nanorattles. About 80% of drugs were released within 5 days. Two factors are considered to concurrently determine the sustained release of Dtxl from silica nanorattles. One is the electro-

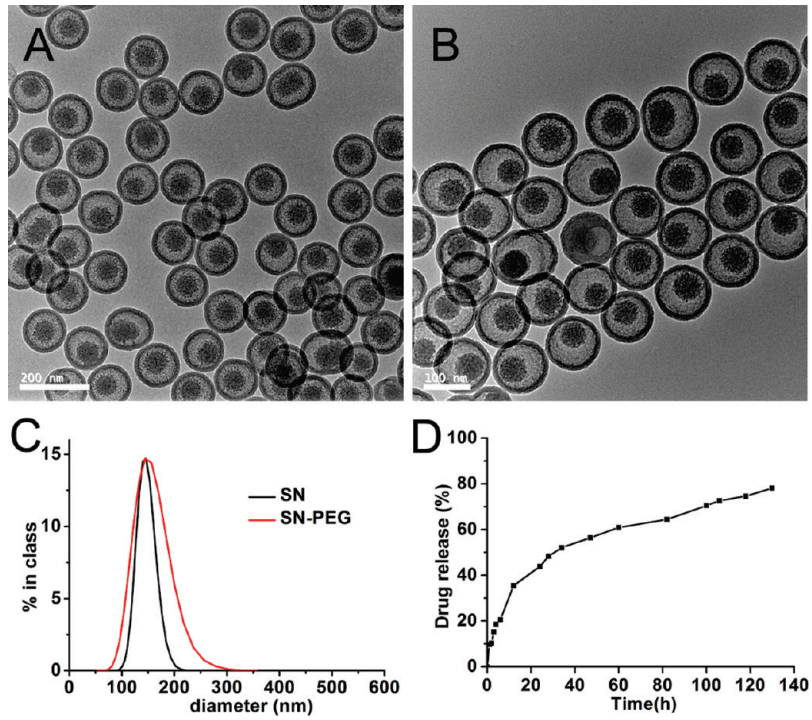

Figure 2. (A) TEM image of silica nanorattle (SN) with a size of 125 nm, (B) TEM image of the silica nanorattles after PEGylation (SN-PEG), (C) size distribution of SN and SN-PEG by dynamic light scattering, and (D) *in vitro* cumulative drug release profile of docetaxel from SN-PEG-Dtxl in neutral PBS medium at 37 °C.

static interaction between the amino group in the matrix of silica nanorattles and the hydroxyl group of Dtxl. The hydrophobic nature of Dtxl is another important reason that decides if the Dtxl would be slowly dissolved from the silica matrix to the release medium.

Efficient cellular internalization of nanoparticles is necessary for intracellular drug delivery and efficient therapy. To monitor the trafficking of SN-PEG intracellularly, luminescent labeled SN (SN@FITC) with high fluorescence was designed and synthesized by incorporating the fluorescent dye of fluorescein isothiocyanate (FITC) into the core of the SN (Figure S2, Supporting Information). The uptake of PEGylated SN@FITC (SN@FITC-PEG) by human liver carcinoma cell of Hep-G2 was evaluated by fluorescence microscopy (Figure 3A−D). After incubating 100 μg/mL of SN@FITC-

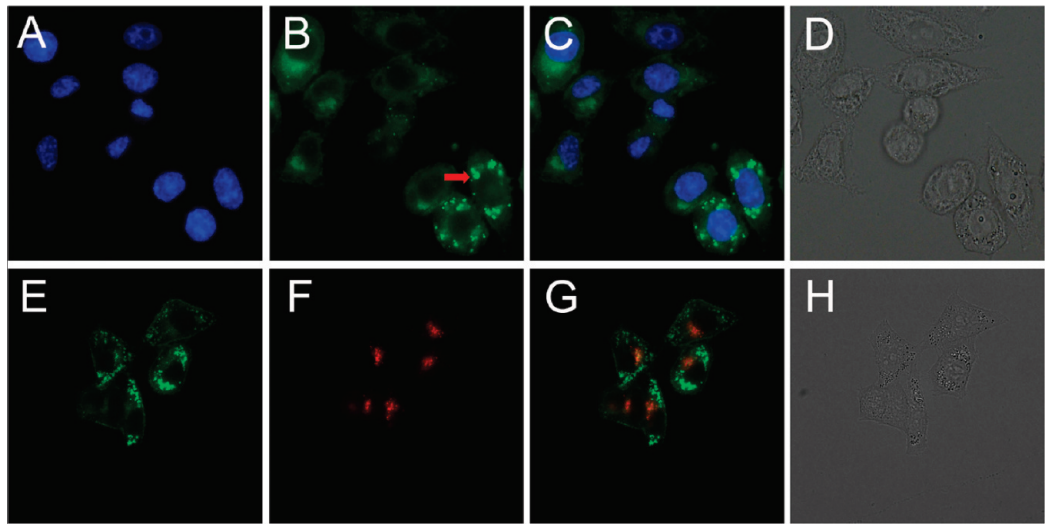

Figure 3. Uptake and subcellular localization of the SN@FITC-PEG in Hep-G2 cells. (A−D) Colocalization of nucleus with SN@FITC-PEG. The cells were incubated with 100 μg/mL of SN-PEG for 4 h, fixed, and then stained with DAPI. (A) Blue fluorescence shows nuclear staining with DAPI. (B) Green fluorescence shows the location of SN@FITC-PEG. (C) Overlaid image of A and B, and (D) corresponding transmission image. (E−H) Colocalization of lysosome with SN@FITC-PEG. The cells were incubated with 100 μg/mL of SN@FITC-PEG for 4 h, washed, and then stained with Lysotracker Red DND-99. (E) Green fluorescence shows the location of SN@FITC-PEG. (F) Red fluorescence shows the location of lysosome (Lysotracker Red DND-99). (G) Overlaid image of E and F, and (H) corresponding transmission image.

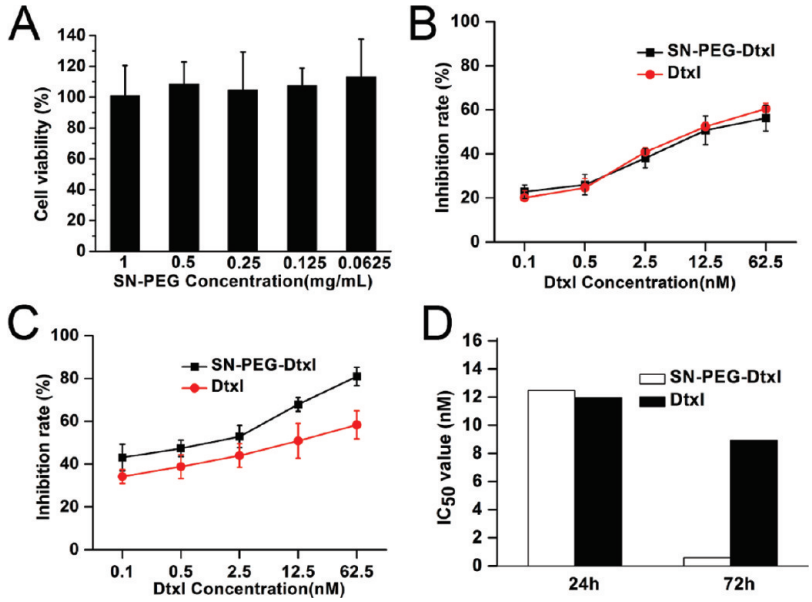

Figure 4. Cytotoxicity of SN-PEG, SN-PEG-Dtxl, and Dtxl on Hep-G2 cells by MTT assays. (A) Cell viability with concentrations of SN-PEG from 0.0625 to 1 mg/mL for 72 h. Inhibition rate of Dtxl and SN-PEG-Dtxl (concentration of Dtxl from 0.1 to 62.5 nM) on Hep-G2 cells for (B) 24 h and (C) 72 h, and (D) corresponding IC_{50} value for 24 and 72 h.

PEG with Hep-G2 cells for 4 h, the cells were fixed and nuclei stained with DAPI (blue). SN@FITC-PEG distributed in almost all of the cells throughout the entire cell cytoplasm (Figure 3B, green fluorescence). In some cells, there were isolated spots of green fluorescence showing higher fluorescence intensities, demonstrating the cluster of the nanorattles (the red arrow in Figure 3B). To distinguish the subcellular location of SN@FITC-PEG, the Hep-G2 cells were incubated with 100 μg/mL of SN@FITC-PEG for 4 h and then stained with Lysotracker Red DND-99 to label the lysosomes (Figure 3E−H). The colocalization between SN@FITC-PEG (green) and lysosome (red) shows that SN@FITC-PEG is rarely colocalized with the lysosomal marker, indicating that the SN@FITC-PEG has a high efficiency to escape from the lysosome to the cytosol. This behavior may be attributed to the "proton sponge" effect, which is important for endosome escape.[27] The results prove that SN-PEG can penetrate the plasma membrane of Hep-G2 cells and translocate into the cytoplasm with high efficiency. In this study, Dtxl is a kind of hydrophobic and membrane-permeable drug that can directly penetrate cell membrane and efficiently enter into the cytoplasm of the cancer cells.[28] For therapy, it does not need a "chaperone" to help it penetrate the cell membrane, but in the case of the membrane-impermeable therapeutic molecules, such as proteins and genes, SNs can facilitate them entering into the cells.[29,30] In another case, for the multi-drug-resistant cells with decreased uptake of chemotherapeutic agents, the silica nanorattles also can act as a transmembrane delivery vehicle to help transport the drug molecules into the cells. Thus it can increase the cell internalization, decrease the drug efflux, and increase the intracellular accumulation of the drugs.[31,32]

The cytotoxicity of the SN-PEG-Dtxl was evaluated and compared with free Dtxl *via* the MTT (3-(4,5-dimethylthiazol-2-yl)-2,5-diphenyltetrazolium bromide) assay. To exclude the possible influence of SN-PEG on cell viability, various concentrations of SN-PEG were incubated for 72 h with Hep-G2 and then cell viability was assessed. Within the tested concentration range even as high as 1 mg/mL, the SN-PEG has no obvious adverse effect on cell viability (Figure 4A), demonstrating the SN-PEG itself has no cytotoxicity. Then, Hep-G2 cells were incubated with a series of equivalent concentrations of free Dtxl or SN-PEG-Dtxl for 24 and 72 h, respectively. Both free Dtxl and SN-PEG-Dtxl showed obvious cell inhibition after 24 or 72 h incubation (Figure 4B,C) with Dtxl concentration from 0.1 to 62.5 nM. For 24 h, the free Dtxl showed similar cytotoxicity to equivalent concentration of SN-PEG-Dtxl in all concentrations. The half-maximum inhibiting concentration (IC_{50} value) of free Dtxl (12 nM) was comparable to that of SN-PEG-Dtxl (12.5 nM) (Figure 4D). For 72 h, SN-PEG-Dtxl exhibited obvious advantage over Dtxl in cytotoxicity in all concentrations. The IC_{50} value of Dtxl (9 nM) and SN-PEG-Dtxl (0.6 nM) decreased to 75 and 4.8% of that at 24 h, respectively. The increased cytotoxicity is contributed from the sustained release of the drug molecules from the SN-PEG and may be contributed from enhanced Dtxl uptake by cells when encapsulated in the SN-PEG.

It is known that docetaxel kills cells *via* stabilizing microtubules, inducing cell-cycle arrest and caspase-2- and caspase-3-dependent apoptosis in breast cancer cells and prostate cancer cells.[33,34] It has also been reported to induce non-apoptosis death (aberrant mitosis) in tumor cells, depending on the dose, cell type, and tumor microenvironment.[35−37] Until now, there have no reports on how docetaxel kills liver cancer cells. In

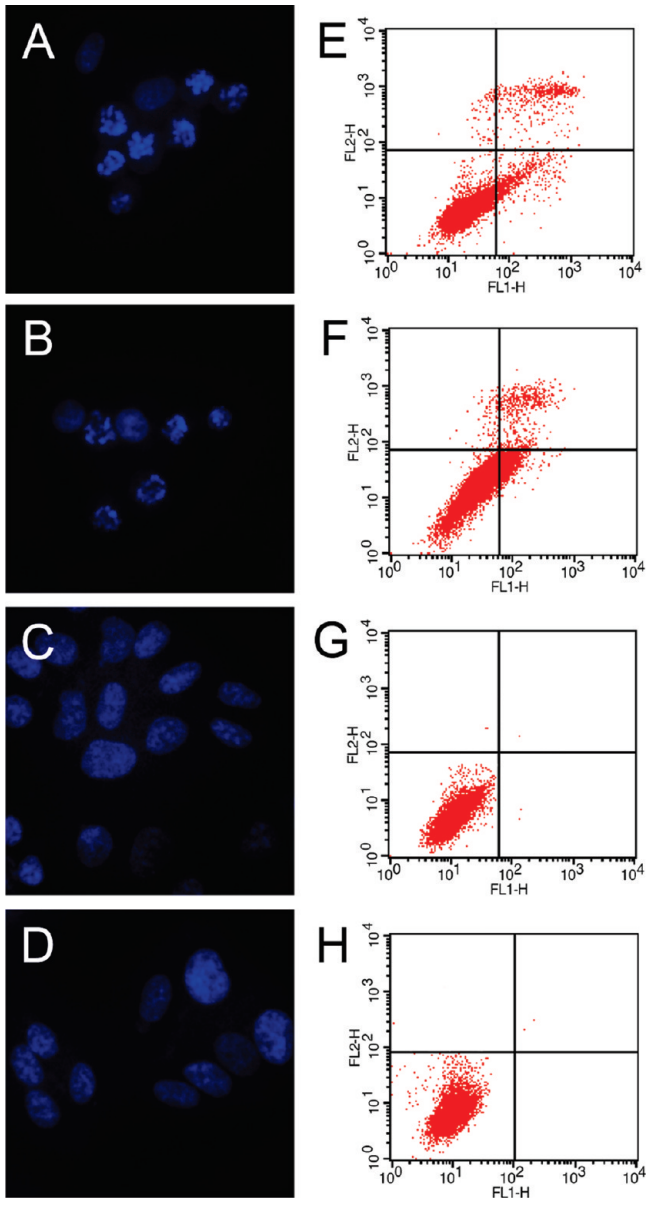

Figure 5. Effect of SN-PEG, SN-PEG-Dtxl, and Dtxl on Hep-G2 apoptosis. Hep-G2 cells were treated with (A) 10 nM Dtxl, (B) SN-Dtxl of 10 nM Dtxl, (C) 100 μg/mL of SN-PEG, and (D) negative control without treatment, and then stained with Hoechst 33258 (blue). Apoptosis was also evaluated after Hep-G2 cells were treated with (E) 10 nM Dtxl, (F) SN-Dtxl of 10 nM Dtxl, (G) 100 μg/mL of SN-PEG, and (H) negative control, and then stained with Annexin-V-FITC and PI. Flow cytometry profile represented Annexin-V-FITC staining on the *X* axis and PI on the *Y* axis.

this study, we first discovered that docetaxel induces Hep-G2 cell death *via* the pathway of apoptosis. The Hep-G2 cells were incubated with Dtxl (10 nM), SN-PEG-Dtxl (10 nM), and SN-PEG (100 μg/mL) for 24 h, fixed with 4% paraformaldehyde, and then stained with Hoechst 33258. Chromatin condensation and apoptotic-body formation can be observed for most of the cells treated with Dtxl (Figure 5A), as well as SN-PEG-Dtxl (Figure 5B). This result indicates that the cytotoxicity of docetaxel on Hep-G2 was induced by apoptosis. Incorporating docetaxel into SN-PEG would not change the apoptosis pathway. The cells treated with a high concentration of SN-PEG (100 μg/mL) (Figure 5C) did not show any abnormality compared to the control (Figure 5D), which further confirms the biocompatibility of SN-PEG. The apoptosis of Hep-G2 induced by Dtxl (10 nM) and SN-PEG-Dtxl (10 nM) was also proven by flow cytometry. The AnnexinV-FITC/PI staining could distinguish early apoptosis from late apoptosis/necrosis cells. In the flow cytometry quadrantal diagram, the lower left, lower right, and upper right quadrants denoted viable, early apoptotic, and late apoptotic/necrotic regions, respectively. Dtxl (Figure 5E) and SN-PEG-Dtxl (Figure 5F) treated cells were found in the lower right quadrant (AnnexinV positive and PI negative) and upper right quadrant (AnnexinV positive and PI positive), confirming cell death by apoptosis. No visible apoptosis and necrosis were observed of the cells treated with SN-PEG (100 μg/mL) (Figure 5G) and control cells (Figure 5H).

Next, we evaluated systematic toxicity of the drug nanocarrier of SN-PEG and the SN-PEG-Dtxl formulation *in vivo*. SN-PEG suspended in saline was injected through the tail vein into ICR mice with a single dose of 40 mg/kg. The gross anatomy and pathomorphology examinations (Figure 6A−D) showed that all of the organs including MPS-related organs of liver (Figure 6A) and spleen (Figure 6B) had no obvious change in morphology including the lymphoid follicles or the area of the white pulp. The result shows that the drug carrier of SN-PEG is biocompatible. The current clinical formulations of docetaxel, Taxotere, have severe adverse effect due to the acute hypersensitive reaction induced by nonionic surfactant polysorbate 80 (Tween-80) and the severe systematic toxicity of Dtxl itself.[26,38] By encapsulating Dtxl into silica nanorattles, the formulation can be readily dispersed in physiological media without any surfactants and cosolvents. To determine the function of SN-PEG for reducing the toxicity of Dtxl clinical formulation, the systematic toxicities of Taxotere and SN-PEG-Dtxl were evaluated in healthy mice. Eighteen healthy female ICR mice with a body weight of about 20 g were randomly divided into three groups, SN-PEG-Dtxl group (20 mg/kg Dtxl), Taxotere group (20 mg/kg Dtxl), and control group (physiological saline). A total of three i.v. administrations (day 1, day 5, and day 9) in a span of 9 days was given. The mice were then kept for another 3 days. Body weight and clinic manifestation were monitored during the course. The mice in the Taxotere group suffered marked weight loss of about 14%, indicating severe toxicity, whereas the mice in the control group and SN-PEG-Dtxl group gained 18 and 13% body weight, respectively (Figure 7A). All the viscera indexes of the SN-PEG-Dtxl group had no obvious change compared with that of control group, whereas the viscera index of liver in the Taxotere groups suffered obvious decrease, demonstrating damage to the liver (Figure S3). Just as reported, Dtxl often has severe

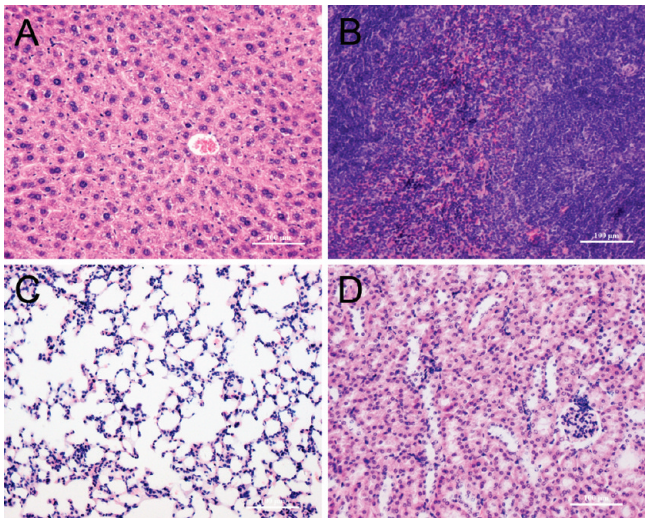

Figure 6. Systematic toxicity of SN-PEG (40 mg/kg, single dose, i.v.) on healthy ICR mice. Histological section of (A) liver, (B) spleen, (C) lung, and (D) kidney stained with H&E. The scale bar is 100 μm.

hematological adverse effects include neutropenia, anemia, and thrombocytopenia. It also can result in significant liver dysfunction.[38,39] Standard hematologic markers of absolute white blood cell count (WBC), lymphocyte count (LyC), monocytes count (MoC), neutrophil count (NeC) and red blood cell count (RBC) were detected and compared among the three groups (Figure 7B). The significant decrease of WBC, MoC, and NeC in the Taxotere group represents the severe hematological toxicity. Although the level of the three markers in the SN-PEG-Dtxl group also decreased compared with that of the control group, the difference compared with the control group was not as significant as that of the Taxotere group. The results indicate that the SN-PEG-Dtxl shows lower toxicity than the Taxotere with equivalent Dtxl concentration. Other hematologic markers including mean corpuscular hemoglobin, platelet count, corpuscular hemoglobin concentration, and mean corpuscular volume had no obvious differences among the three groups (data not shown). The biochemical markers for liver function including alanine aminotransferase (ALT), aspartate aminotransferase (AST), and total bilirubin (TBIL) were also analyzed (Figure S4A−C). The predominant increase in ALT and AST activity in the Taxotere group indicates severe liver injury. Both Taxotere and SN-PEG-Dtxl had no obvious adverse influence on the plasma creatinine (CRE) and urea nitrogen (BUN) that represent kidney function (Figure S4D,E). The histology results also indicate that the liver has no obvious histopathological abnormalities in the SN-PEG-Dtxl group relative to the control (Figure 7C), but in the Taxotere group, 5 of 6 mice had remarkable microgranuloma formation in the livers (Figure 7D, red arrow). It is estimated that the necrosis of liver cells induced by Dtxl recruits the monocytes and kupffers to the location. Other tissues including spleen, lung, and kidney have no obvious histopathological abnormalities or lesions in all groups (Figure S5). All of these results prove that the SN-PEG-Dtxl has lower systematic toxicity compared with Taxotere. It can be possibly attributed to three points. First, the sequestration of Dtxl by SN-PEG-Dtxl reduces the liver toxicity by reducing the systemic concentration of free Dtxl. Second, the drug delivery system of SN-PEG

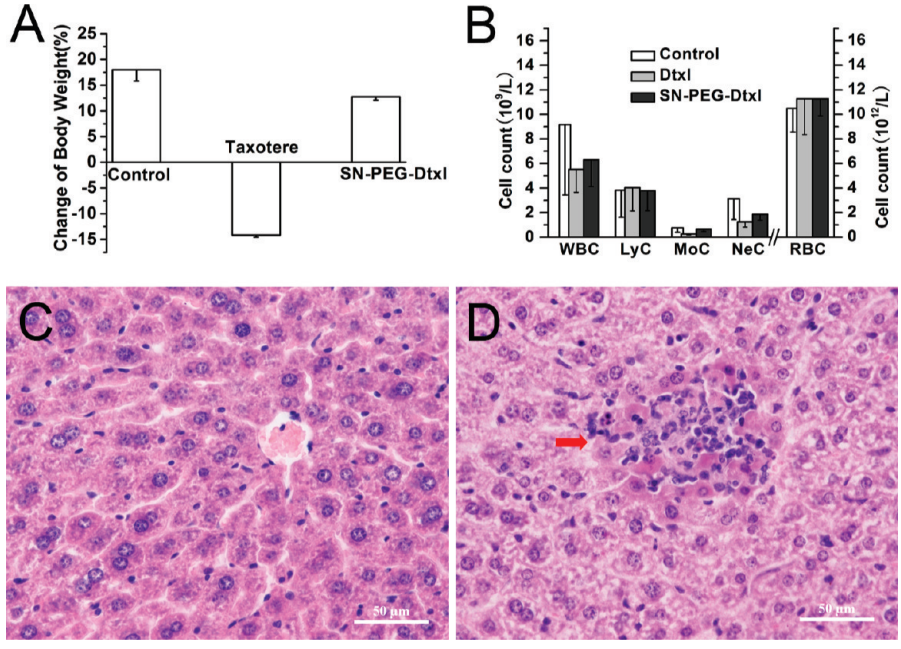

Figure 7. Systematic toxicity of Taxotere and SN-PEG-Dtxl (20 mg/kg, three doses, i.v.) on healthy ICR mice. (A) Change of body weight, (B) values of hematological markers, and histological section stained with H&E of liver samples of (C) SN-PEG-Dtxl and (D) Taxotere group.

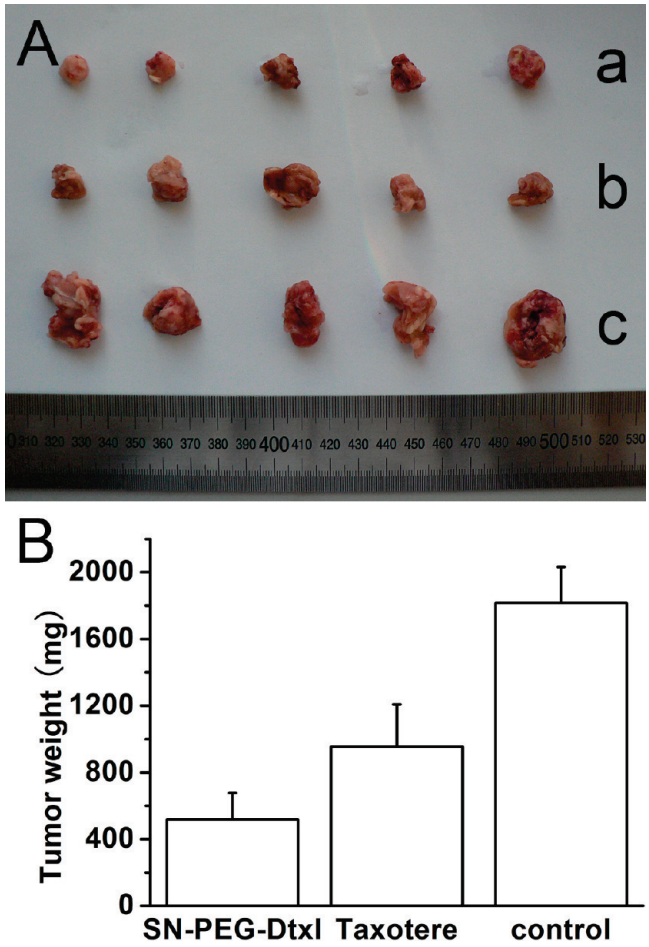

Figure 8. ***In vivo*** **antitumor activities of SN-PEG-Dtxl and Taxotere on H22 liver cancer subcutaneous model (20 mg/kg of Dtxl, four doses, i.v.). (A) Photographs of tumors from (a) SN-PEG-Dtxl group, (b) Taxotere group, and (c) control group with saline. (B) Tumor sizes of each group.**

with good biocompatibility can be readily suspended in the injection media without any toxic excipients such as Tween-80. Last, the PEGylated SN with suitable size may have decreased accumulation in and more rapid clearance from organs.[40]

In vivo therapeutic efficacy for liver cancer was assessed using the marine hepatocarcinoma 22 (H22) subcutaneous model. Fifteen tumor-bearing ICR female mice with tumor size of about 200 mm^3 at the right flank were divided into three groups, (a) SN-PEG-Dtxl group (20 mg/kg Dtxl), (b) Taxotere group (20 mg/kg Dtxl), and (c) control group (physiological saline) with minimal weight and tumor size differences. The drugs were intravenously administered (i.v.) through the tail vein every 4 days (day 1, day 5, day 9, and day 13) for a total of four times. No mice died during the course of therapy. By the planned end point of day 17, all of the animals were euthanized to evaluate the tumor sizes and inhibition rates. The picture of tumors excised from the mice of each group (Figure 8A) showed that the tumor sizes of both of the Taxotere and SN-PEG-Dtxl group were visibly smaller than that of the control group, which means tumor inhibition for both groups (Figure 8B), but the tumors in the SN-Dtxl group were smaller than that in the Taxotere group. The average inhibition rate calculated from tumor weight by Taxotere was about 57%, while that of the SN-PEG-Dtxl group was as high as 72%. Although liver cancer is resistant to most anticancer drugs, our results here prove that the Dtxl has a high suppression effect on Hep-G2 cells and H22 liver cancer. The enhanced tumor inhibition of the SN-Dtxl may be attributed to the sustained Dtxl release from SN-PEG *in vivo* and as well as the accumulation of drug-loaded SN in the intratumor due to EPR effect once intravenously administered. It is believed by further bioconjugating the SN with cancer-specific targeting ligands (for example, antibody, peptide, and aptermer), the specificity of the delivery system for cancer cells and the therapeutic efficacy can be further enhanced.[10,20]

CONCLUSION

In summary, this study represents a significant progress of *in vivo* cancer therapy with mesoporous silica nanomaterials. The silica nanorattles show advantages for *in vivo* enhancement of therapy efficacy and reducing the systematic toxicity of the antitumor drugs. It has the potential to be developed as a versatile and robust drug delivery platform for accommodating a wide range of therapy modalities with high drug loading amount, including hydrophobic and hydrophilic pharmaceutical drugs, siRNA, and therapeutic proteins. Notwithstanding future challenges about their long-term biocompatibility, the present data provide a pathway for the application of the mesoporous silica nanomaterials as an efficient drug carrier. We believe our preliminary work would promote further understanding of other silica mesoporous nanomaterials and pave the way for future clinical translation.

EXPERIMENTAL METHOD

Synthesis and PEGylation of Silica Nanorattle. SN and SN@FITC of about 125 nm were fabricated *via* a modified Stöber reaction according to our previously reported method.[23] For PEGylation, 1 g of silica nanorattles was mixed with 200 mg of mPEG-SC (methoxypoly(ethylene glycol)succinimidyl carbonate) (4 KD, Kaizheng Biotech., Beijing) and reacted for 4 h at room temperature, and then the unreacted molecules were removed by repeated centrifugation.

In Vitro **Drug Loading and Release.** To load Dtxl (Sanwei Pharmaceutical., Shanghai) into the pores of the particles, SN-PEG was dispersed in a solution of Dtxl (40 mg/mL in ethanol) and stirred for 24 h, followed by centrifugation and washing extensively with PBS to obtain the drug-loaded SN-PEG (SN-PEG-Dtxl). For drug release assay, the SN-PEG-Dtxl samples were placed in dialysis tubing (10 000 Da) and immersed in 20 mL of release medium, stirring at room temperature. The release medium (8 mL) was taken at given time intervals. The concentration of Dtxl was determined by UV/vis spectroscopy measurements at a wave-

length of 230 nm. Drug loading amount was calculated according to the equation of drug loading amount (%) = 100 × W_{Dtxl}/($W_{SN\text{-}PEG\text{-}Dtxl}$), where W_{Dtxl} is the weight of Dtxl loaded into the nanorattle, and $W_{SN\text{-}PEG\text{-}Dtxl}$ is the weight of SN-PEG-Dtxl.

Cellular Uptake and Internalization. Human liver carcinoma cells of Hep-G2 cells (ATCC) were maintained in high glucose Dulbecco's modified Eagle's medium (DMEM) (Gibco), supplemented with 10% FBS (Hyclone) at 37 °C in a humidified atmosphere of 5% CO_2. The cell culture media were supplemented with 100 units/mL penicillin and 100 μg/mL streptomycin. The Hep-G2 cells were seeded on glass-bottom dishes (35 mm, kindly provided by MatTek Corporation). A final concentration of 100 μg/mL SN@FITC-PEG was added to the cells and incubated for 4 h. The cells were washed with PBS three times, fixed with 4% paraformaldehyde, and then stained with 10 μg/mL DAPI (2-(4-amidinophenyl)-6-indolecarbamidine dihydrochloride, Sigma). Micrographs were taken on a Nikon fluorescence microscope (Nikon Eclipse Ti-S, CCD: Ri1). For colocalization with lysosome, the cells were coincubated with 100 μg/mL of SN@FITC-PEG for 4 h, and then washed, stained with 60 nM Lysotracker Red DND-99 (Beyotime Institute of Biotechnology, Haimen, China) for 1 h, and observed on a fluorescence microscope.

***In Vitro* Cell Viability.** The cytotoxicity of SN-PEG, SN-PEG-Dtxl, and Dtxl was evaluated by MTT viability assay. Dtxl was dissolved using DMSO, and the final concentration of DMSO in culture media was less than 0.5%. For 24 h detection, the cells were seeded at a density of 8000 cells/well on 96-well plates (Costar), and for 72 h detection, the cell density was 2000 cells/well. After incubating the cells with silica nanorattles, Dtxl, and SN-PEG-Dtxl for 24 h (or 72 h), MTT (3-(4,5-dimethylthiazol-2-yl)-2,5-diphenyltetrazolium bromide) (Sigma) (final concentration of 0.5 mg/mL) was added to each well. After 4 h of incubation at 37 °C, colorimetric measurements were performed at 570 nm on a scanning multiwell spectrometer (Multiskan MK3 Thermo labsystems). Data were expressed as mean ± standard deviation (SD) of at least six independent experiments.

Cell Apoptosis Assays. The cell apoptosis was detected by assessment of nuclear morphology staining with Hoechst 33258. Cells were treated with SN-PEG (100 μg/mL), SN-PEG-Dtxl (10 nM), and Dtxl (10 nM) for 24 h. Then the cells were washed and fixed with 4% paraformaldehyde. After being stained with the fluorescent probe of Hoechst 33258 (Sigma) (10 μg/mL) at room temperature for 10 min, the cells were observed on a fluorescence microscope. Cell apoptosis was also determined by FACS with an AnnexinV-FITC apoptosis detection kit. Hep-G2 cells were seeded at 5 × 10^5 cells in 6-well plates and incubated with SN-PEG (100 μg/mL), SN-PEG-Dtxl (10 nM), and Dtxl (10 nM) for 24 h. The cells were washed with PBS, resuspended in binding buffer, and incubated with Annexin V and PI at room temperature for 10 min and then analyzed immediately using the FACSCalibur system (Becton Dickinson) with CellQuest software.

***In Vivo* Systematic Toxicity.** ICR mice (purchased from Vital River Corp., Beijing) weighing 18 ± 2 g were kept in an environment complying with the NIH guidelines for the care and use of laboratory animals. All animal procedures were performed following protocol approved by the Institutional Animal Care. A total of 18 healthy female ICR mice were allocated to three groups and intravenously administrated with (a) SN-PEG-Dtxl (Dtxl of 20 mg/kg, 200 μL, dispersed in saline), (b) Taxotere (Dtxl of 20 mg/kg, 200 μL, dispersed in saline), and (c) control group (200 μL saline) every 4 days (day 1, day 5, and day 9) through tail veins until a total of three administrations were completed. Body weights and clinic manifestation were observed and recorded carefully throughout the experiment period. On day 12, blood samples were collected from the ocular vein (about 0.8−1 mL each mouse) and centrifuged twice at 3000 rpm for 10 min to separate serum. The coefficients of liver, kidneys, and spleen to body weight were calculated as the ratio of tissues (wet weight, mg) to body weight (g). Tissues recovered from the necropsy were fixed in 10% formalin, embedded in paraffin, sectioned, and stained with hematoxylin and eosin (H&E) for histological examination using standard techniques. After hematoxylin/eosin staining, the slides were observed and photos were taken using an optical microscope.

***In Vivo* Antitumor Effect.** The female mice were injected subcutaneously in the right axillary region with 0.1 mL of cell suspension containing 5 × 10^6 hepatoma 22 (H22) cells (ATCC). After tumor size had reached about 200 mm^3, the mice were divided into three groups (n = 5), minimizing weight and tumor size differences. The mice were intravenously administered with (a) Taxotere (20 mg/kg, 200 μL, diluted with saline), (b) SN-PEG-Dtxl (20 mg/kg Dtxl, 200 μL, dispersed in saline), and (c) saline (200 μL) (control group) every 4 days through tail veins (day 1, day 5, day 9, and day 13). On day 17, after four times of therapy, all of the animals were euthanized, and the tumors were dissected and weighed. Tumor growth inhibition rates were calculated using the formula inhibition (%) = 100 × (C − T)/C, where C is the average tumor weight of the control group and T the average tumor weight of each treated group.

Acknowledgment. The work was financially supported by National Natural Science Foundation of China (Nos. 60736001, 30900349, 30800258), the National Hi-Tech Research and Development Program ('863' Program) of China (No. 2007AA021803, No. 2007AA021802), and Innovation Foundation of the Chinese Academy of Sciences (KJCX2.YW.M03).

Supporting Information Available: Zeta potential of silica nanorattle before and after PEGylation, properties of SN@FITC, details about systematic toxicity of Taxotere and SN-PEG-Dtxl, graphs showing *in vivo* therapeutic efficacy on H22 are available. This material is available free of charge *via* the Internet at http://pubs.acs.org.

REFERENCES AND NOTES

1. Vallet-Regi, M.; Rámila, A.; del Real, R. P.; Pérez-Pariente, J. A New Property of MCM-41: Drug Delivery System. *Chem. Mater.* **2001**, *13*, 308–311.
2. Slowing, I. I.; Trewyn, B. G.; Giri, S.; Lin, V. S. Y. Mesoporous Silica Nanoparticles for Drug Delivery and Biosensing Applications. *Adv. Funct. Mater.* **2007**, *17*, 1225–1236.
3. Nan, A.; Bai, X; Son, S. J.; Lee, S. B.; Ghandehari, H. Cellular Uptake and Cytotoxicity of Silica Nanotubes. *Nano Lett.* **2008**, *8*, 2150–2154.
4. Piao, Y.; Burns, A.; Kim, J.; Wiesner, U.; Hyeon, T. Designed Fabrication of Silica-Based Nanostructured Particle Systems for Nanomedicine Applications. *Adv. Funct. Mater.* **2008**, *18*, 3745–3758.
5. Mal, N. K.; Fujiwara, M.; Tanaka, Y. Photocontrolled Reversible Release of Guest Molecules from Coumarin Modified Mesoporous Silica. *Nature* **2003**, *421*, 350–353.
6. Torney, F.; Trewyn, B. G.; Lin, V. S. Y.; Wang, K. Mesoporous Silica Nanoparticles Deliver DNA and Chemicals into Plants. *Nat. Nanotechnol.* **2007**, *2*, 295–300.
7. Lai, C. Y.; Trewyn, B. G.; Jeftinija, D. M.; Jeftinija, K.; Xu, S.; Jeftinija, S.; Lin, V. S. Y. A Mesoporous Silica Nanosphere-Based Carrier System with Chemically Removable CdS Nanoparticle Caps for Stimuli-Responsive Controlled Release of Neurotransmitters and Drug Molecules. *J. Am. Chem. Soc.* **2003**, *125*, 4451–4459.
8. Lu, J.; Liong, M.; Zink, J. I.; Tamanoi, F. Mesoporous Silica Nanoparticles as a Delivery System for Hydrophobic Anticancer Drugs. *Small* **2007**, *3*, 1341–1346.
9. Chen, A. M.; Zhang, M.; Wei, D. G.; Stueber, D.; Taratula, O.; Minko, T.; He, H. X. Co-delivery of Doxorubicin and Bcl-2 siRNA by Mesoporous Silica Nanoparticles Enhances the Efficacy of Chemotherapy in Multidrug-Resistant Cancer Cells. *Small* **2009**, *5*, 2673–2677.
10. Rosenholm, J. M.; Peuhu, E.; Eriksson, J. E.; Sahlgren, C.; Lindén, M. Targeted Intracellular Delivery of Hydrophobic Agents Using Mesoporous Hybrid Silica Nanoparticles as Carrier Systems. *Nano Lett.* **2009**, *9*, 3308–3311.
11. Lou, X. W.; Archer, L. A.; Yang, Z. C. Hollow Micro-/Nanostructures: Synthesis and Applications. *Adv. Mater.* **2008**, *20*, 3987–4019.

12. Chen, Y.; Chen, H. R.; Guo, L. M.; He, Q. J.; Chen, F.; Zhou, J.; Feng, J. W.; Shi, J. L. Hollow/Rattle-Type Mesoporous Nanostructures by a Structural Difference-Based Selective Etching Strategy. *ACS Nano* **2010**, *4*, 529–539.
13. Zhu, Y. F.; Ikoma, T.; Hanagata, N.; Kaskel, S. Rattle-Type Fe_3O_4@SiO_2 Hollow Mesoporous Spheres as Carriers for Drug Delivery. *Small* **2009**, *6*, 471–478.
14. Suh, H. W.; Ram, J. A.; Suh, Y. H.; Suslick, K. S. Porous, Hollow, and Ball-in-Ball Metal Oxide Microspheres: Preparation, Endocytosis, and Cytotoxicity. *Adv. Mater.* **2006**, *18*, 1832–1837.
15. Lu, J.; Liong, M.; Li, Z.; Zink, J. I.; Tamanoi, F. Biocompatibility, Biodistribution, and Drug-Delivery Efficiency of Mesoporous Silica Nanoparticles for Cancer Therapy in Animals. *Small* **2010**, *6*, 1794–1805.
16. Schipper, M.; Nakayama-Ratchford, N.; Davis, C.; Kam, N.; Chu, P.; Liu, Z.; Sun, X.; Dai, H.; Gambhir, S. A Pilot Toxicology Study of Single-Walled Carbon Nanotubes in a Small Sample of Mice. *Nat. Nanotechnol.* **2008**, *3*, 216–221.
17. Park, J. H.; Gu, L.; von Maltzahn, G.; Ruoslahti, E.; Bhatia, S. N.; Sailor, M. J. Biodegradable Luminescent Porous Silicon Nanoparticles for *In Vivo* Applications. *Nat. Mater.* **2009**, *8*, 331–336.
18. Moghimi, S. M.; Hunter, A. C.; Murray, J. C. Long-Circulating and Target-Specific Nanoparticles: Theory to Practice. *Pharmacol. Rev.* **2001**, *53*, 283–318.
19. Owens III, D. E.; Peppas, N. A. Opsonization, Biodistribution, and Pharmacokinetics of Polymeric Nanoparticles. *Int. J. Pharm.* **2006**, *307*, 93–102.
20. Rosenholm, J. M.; Meinander, A.; Peuhu, E.; Niemi, R.; Eriksson, J. E.; Sahlgren, C.; Lindén, M. Targeting of Porous Hybrid Silica Nanoparticles to Cancer Cells. *ACS Nano* **2009**, *3*, 197–206.
21. Iyer, A. K.; Khaled, G.; Fang, J.; Maeda, H. Exploiting the Enhanced Permeability and Retention Effect for Tumor Targeting. *Drug Discovery Today* **2006**, *11*, 812–818.
22. Maeda, H.; Wu, J.; Sawa, T.; Matsumura, Y.; Hori, K. Tumor Vascular Permeability and the EPR Effect in Macromolecular Therapeutics: A Review. *J. Controlled Release* **2000**, *65*, 271–284.
23. Chen, D.; Li, L. L.; Tang, F. Q.; Qi, S. Facile and Scalable Synthesis of Tailored Silica "Nanorattle" Structures. *Adv. Mater.* **2009**, *21*, 3804–3807.
24. Milton Harris, J.; Chess, R. B. Effect of Pegylation on Pharmaceuticals. *Nat. Rev. Drug Discovery* **2003**, *2*, 214–221.
25. Otsuka, H.; Nagasaki, Y.; Kataoka, K. PEGylated Nanoparticles for Biological and Pharmaceutical Applications. *Adv. Drug Delivery Rev.* **2003**, *55*, 403–419.
26. Montero, A.; Fossella, F.; Hortobagyi, G.; Valero, V. Docetaxel for Treatment of Solid Tumours: A Systematic Review of Clinical Data. *Lancet Oncol.* **2005**, *6*, 229–239.
27. Boussif, O.; Lezoualc'h, F.; Zanta, M. A.; Mergny, M. D.; Scherman, D.; Demeneix, B.; Behr, J. P. A Versatile Vector for Gene and Oligonucleotide Transfer into Cells in Culture and *In Vivo*: Polyethylenimine. *Proc. Natl. Acad. Sci. U.S.A.* **1995**, *92*, 7297–7301.
28. Farokhzad, O. C.; Cheng, J. J.; Teply, B. A.; Sherifi, I.; Jon, S.; Kantoff, P. W.; Richie, J. P.; Langer, R. Targeted Nanoparticle-Aptamer Bioconjugates for Cancer Chemotherapy *In Vivo*. *Proc. Natl. Acad. Sci. U.S.A.* **2006**, *103*, 6315–6320.
29. Slowing, I. I.; Trewyn, B. G.; Lin, V. S. Y. Mesoporous Silica Nanoparticles for Intracellular Delivery of Membrane-Impermeable Proteins. *J. Am. Chem. Soc.* **2007**, *129*, 8845–8849.
30. Xia, T.; Kovochich, M.; Liong, M.; Meng, H.; Kabehie, S.; George, S.; Zink, J. I.; Nel, A. E. Polyethyleneimine Coating Enhances the Cellular Uptake of Mesoporous Silica Nanoparticles and Allows Safe Delivery of siRNA and DNA Constructs. *ACS Nano* **2009**, *3*, 3273–3286.
31. Gottesman, M. M.; Fojo, T.; Bates, S. E. Multidrug Resistance in Cancer: Role of ATP-Dependent Transporters. *Nat. Rev. Cancer* **2002**, *2*, 48–58.
32. Susa, M.; Iyer, A. K.; Ryu, K.; Hornicek, F. J.; Mankin, H.; Amiji, M. M.; Duan, Z. F. Doxorubicin Loaded Polymeric Nanoparticulate Delivery System to Overcome Drug Resistance in Osteosarcoma. *BMC Cancer* **2009**, *9*, 399.
33. Rowinsky, E. K. The Development and Clinical Utility of the Taxane Class of Antimicrotubule Chemtherapy Agents. *Annu. Rev. Med.* **1997**, *48*, 353–374.
34. Wang, L. G.; Liu, X. M.; Kreis, W.; Budman, D. R. The Effect of Antimicrotubule Agents on Signal Transduction Pathways of Apoptosis: A Review. *Cancer Chemother. Pharmacol.* **1999**, *44*, 355–361.
35. Morse, D. L.; Gray, H.; Payne, C. M.; Gillies, R. J. Docetaxel Induces Cell Death through Mitotic Catastrophe in Human Breast Cancer Cells. *Mol. Cancer Ther.* **2005**, *4*, 1495–1504.
36. Schimming, R.; Mason, K. A.; Hunter, N.; Weil, M.; Kishi, K.; Milas, L. Lack of Correlation between Mitotic Arrest or Apoptosis and Antitumor Effect of Docetaxel. *Cancer Chemother. Pharmacol.* **1999**, *43*, 165–172.
37. Airoldi, M.; Cattel, L.; Pedani, F.; Marchionatti, S.; Tagini, V.; Bumma, C.; Recalenda, V. Clinical and Pharmacokinetic Data of a Docetaxel-Epirubicin Combination in Metastatic Breast Cancer. *Breast Cancer Res. Treat.* **2001**, *70*, 185–195.
38. Caponigro, F.; Longo, F.; Perri, F.; Ionna, F. Docetaxel in the Management of Head and Neck Cancer. *Anticancer Drugs* **2009**, *20*, 639–645.
39. Lavelle, F.; Bissery, M. C.; Combeau, C.; Riou, J. F.; Vrignaud, P.; André, S. Preclinical Evaluation of Docetaxel (Taxotere). *Semin. Oncol.* **1995**, *22*, 3–16.
40. Liu, Z.; Davis, C.; Cai, W. B.; He, L. N.; Chen, X. Y.; Dai, H. J. Circulation and Long-Term Fate of Functionalized, Biocompatible Single-Walled Carbon Nanotubes in Mice Probed by Raman Spectroscopy. *Proc. Natl. Acad. Sci. U.S.A.* **2008**, *105*, 1410–1415.